RSC Advances

ROYAL SOCIETY OF CHEMISTRY

www.rsc.org/advances

RSC Advances

Communication

One-step melamine-assisted synthesis of graphene-supported AuPt@Au nanocrystals for enhanced catalytic reduction of *p*-nitrophenol

Received 00th January 20xx,
Accepted 00th January 20xx

DOI: 10.1039/x0xx00000x

www.rsc.org/

Qi Liu,[a] Yan-Ru Xu,[a] Ai-Jun Wang,[a b] Jiu-Ju Feng [a b]*

Abstract: In this work, monodispersed core-shell AuPt@Au nanocrystals supported on reduced graphene oxide (AuPt@Au NCs/rGO) were fabricated by a one-step wet-chemical approach using melamine as a structure-director and stabilizing agent. Transmission electron microscopy (TEM), high-angle annular dark-field scanning TEM (HAADF-STEM), X-r diffraction (XRD), X-ray photoelectron spectroscopy (XPS) and selected-area electron diffraction (SAED) were employed to examine their structure and morphology. The as-synthesized nanocomposites displayed better catalytic activity for p nitrophenol reduction and improved reusability as compared with monometallic Au/rGO, Pt/rGO and commercial Pt/C catalysts.

1. Introduction

Bimetallic nanomaterials are researched extensively for their superior electronic, catalytic and optical properties over monometallic counterparts, thanks to the synergetic effects between the two individual metals,[1, 2] along with the widespread applications in catalysis,[3, 4] drug delivery,[5] plasmonics,[6] sensors[7] and surface enhanced Raman scattering (SERS).[8] Furthermore, the properties of the bimetals are tightly determined by the particle size, shape and structure.[2, 9] Therefore, shape-controlled synthesis of bimetallic nanocrystals (NCs) has attracted significant attention recently.[10, 11]

To date, bimetallic nanostructures with a variety of morphologies (e.g., dendrites,[12] wires,[13] polyhedrons[14] and cages[15]) have been synthesized by hydrothermal,[4] radiation,[16] wet chemical reduction[17] and electrochemical deposition.[18] Among them, wet chemical reduction possesses the merits of low cost, simplicity and feasibility, and thereby many nanostructures were prepared by reducing the metal salt precursors from aqueous phase.[19, 20]

Graphene attracts tremendous interest in material, chemistry and physics because of its enlarged theoretical surface area, high electrical conductivity, good thermal/chemical stability and strong mechanical strength.[21-23] As a result, graphene are widely explored in sensors,[24] hydrogen storage devices,[25] transistors[26] and catalysis.[27]

Impressively, graphene is emerging as good support for immobilizing and dispersing metallic nanocatalysts.[28] The existence of graphene can maximize the specific surface area of the attached catalyst and prevent its aggregation, which are important to improve and maintain the catalytic activity of the catalyst.[27]

p-Nitrophenol is a water pollutant, which has good chemical, biological stability, high toxicity and been listed as one of "priority pollutant" by US Environmental Protection Agency.[29] Hence, many methods were developed for its reduction and/or oxidative degradation. For example, Fenton reactions are usually used for the oxidative degradation of *p*-nitrophenol to reduce chemical oxygen demand (COD) and many transition-metal-based Fenton-like catalysts are prepared.[30, 31] Recently, the catalytic reduction of *p*-nitrophenol in aqueous solution with sodium borohydride ($NaBH_4$) supplies an alternative facile and green method to solve such environmental problem and gains increasing attention.[29, 32] Furthermore, the reduction product (*p*-aminophenol) is a vital intermediate in the manufacture of pharmaceuticals, plasticizers, dyes and hair-dyeing agent.[33, 34] Therefore, many metallic catalysts including Ni, Cu and noble metals were introduced to the catalytic reduction of *p*-nitrophenol in the literature lately.[12, 29, 34, 35]

Herein, a one-step wet-chemical approach was developed to prepare reduced graphene oxide-supported AuPt@Au nanocrystals (AuPt@Au NCs/rGO) in the presence of melamine. The catalytic performance of the as-obtained nanocomposites was examined by the reduction of *p*-nitrophenol to *p*-aminophenol with $NaBH_4$ in aqueous media.

[a] School of Chemistry and Chemical Engineering, Henan Normal University, Xinxiang, 453007, China
[b] College of Chemistry and Life Science, College of Geography and Environmental Science, Zhejiang Normal University, Jinhua, 321004, China
*Corresponding author: jjfeng@zjnu.cn; Tel./Fax: +86 579 82282269.
Electronic Supplementary Information (ESI) available: [details of any supplementary information available should be included here]. See DOI: 10.1039/x0xx00000x

2. Experimental

2. 1 Synthesis of AuPt@Au NCs/rGO

Reduced graphene oxide (rGO) were firstly prepared from graphite powder based on the modified Hummer's method,[28, 36] followed by the ultrasonication for at least 0.5 h before use. For typical synthesis of AuPt@Au NCs/rGO, the precursors of $HAuCl_4$ and H_2PtCl_6 were subsequently injected into the suspension of graphene oxide (GO) in the presence of melamine under stirring, followed by the drop-wisely addition of hydrazine hydrate solution under constant stirring at 60 °C. The details of the experiments were provided in Supporting Information (SI).

2.2 Catalytic reduction of *p*-nitrophenol

In a typical catalytic procedure, 1 mL of the freshly-prepared $NaBH_4$ solution (0.5 M) and 500 µL of *p*-nitrophenol (0.7 mM) were subsequently put into 1 mL of water. The reduction can not proceed in the absence of AuPt@Au NCs/rGO. To intrigue the catalytic reaction, different amounts of AuPt@Au NCs/rGO (1 g L^{-1}) were added to the reacted media. The reaction progress was monitored by using UV-vis spectrophotometer (Lambda 950, Perkin Elmer Corporation) over a scanning range of 250-550 nm. For comparison, commercial Pt/C, monometallic Au/rGO and Pt/rGO were investigated as referenced materials.

In recycling tests, AuPt@Au NCs/rGO was collected, cleaned, and used repeatedly for subsequent reaction under the same conditions, similar to the previous work.[35, 37]

3. Results and discussion

3. 1 Characterization

Fig. 1 shows the representative transmission electron microscopy (TEM) and high-resolution TEM (HR-TEM) images of the typical sample. **Fig. 1A** clearly shows the wrinkled rGOs, accompanied with the emergence of many dendritic nanospheres on rGO surface, confirming the deposition of AuPt@Au NCs on rGO. These observations are different from Au/rGO with much large irregular solid nanospheres and Pt/rGO with small aggregated solid nanoparticles (**Fig. S1, SI**).

The selective area electron diffraction (SAED) pattern (**inset in Fig. 1B**) reveals good polycrystalline structure of AuPt@Au NCs. More information is provided by HR-TEM images (**Fig. 1C-E**), displaying the well-resolved lattice fringes with interplanar spacing distances of 0.227, 0.231 and 0.201 nm from the marked positions, in accordance with the (111) and (200) planes of the face-centered-cubic (fcc) AuPt@Au NCs,[38-40] respectively.

The core-shell structure of AuPt@Au NCs was verified by high-angle annular dark-field scanning transmission electron microscopy-energy dispersive X-ray spectroscopy (HAADF-STEM-EDS). As can be seen from **Fig. 2A-C**, the average size of Au nanosphere (75 nm) is larger than that of Pt nanosphere (68 nm). The line scanning image (**Fig. 2D**) also evidences the core-shell structure with an Au-Pt alloy as core and an exterior Au-rich shell. The molar ratio of At to Pt is estimated to be

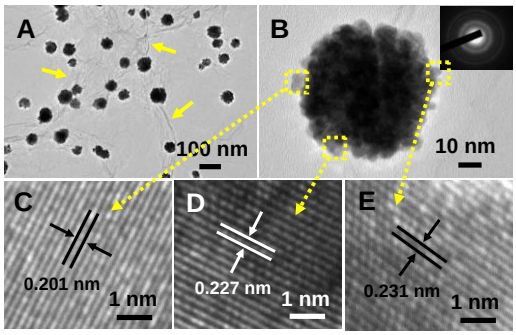

Fig. 1. TEM (A) and HR-TEM (B-E) images of AuPt@Au NCs/rGO. Inset in B shows the corresponding SAED pattern. Arrows in (A) indicate the wrinkles of rGO.

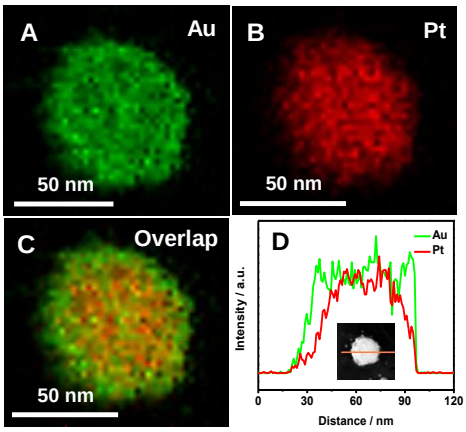

Fig. 2. HAADF-STEM-EDS mapping images (A-C) and scanning profiles (D) of AuPt@Au NCs. Inset in (D) shows the corresponding HAADF-STEM image.

56.3:43.7 on the basis of the EDS analysis (**Fig. S2, SI**). This value is close to the stoichiometric ratio (1:1) of the precursors, reflecting the complete reduction of all the metal precursors.

Fig. 3 shows X-ray diffraction (XRD) patterns of AuPt@Au NCs/rGO and GO. The XRD spectrum of AuPt@Au NCs/rGO shows the characteristic diffraction peaks at 39.6°, 45.2°, 66.3°, and 79.5°, reflecting the fcc structure.[38] These peaks locate between those of single Au (JCPDS-04-0784) and Pt (JCPDS-04-0802), owing to the presence of AuPt alloy as the core.[41] Meanwhile, the representative diffraction peak of GO at 11° vanishes in the case of AuPt@Au NCs/rGO, while a new broad peak appears at 23°, revealing the effective reduction of GO in the synthetic process.[27]

X-ray photoelectron spectroscopy (XPS) was employed to examine the surface compositions of AuPt@Au NCs/rGO. In the survey spectrum (**Fig. 4A**), the dominant XPS peaks at 71, 84, 284, 399 and 532 eV come from Pt, Au, C, N and O elements.

High-resolution XPS spectra of Au 4f, Pt 4f and C 1s are provided for detail information (**Fig. 4B-D**). Clearly, the Au 4f peak is deconvoluted into two peaks at 83.73 and 87.40 eV,

which are contributed to metallic Au^0.[42] As to Pt 4f spectrum, there are two pairs of peaks. The stronger pair at 70.57 and 73.91 eV is indexed to metallic Pt^0, while the minor couple at

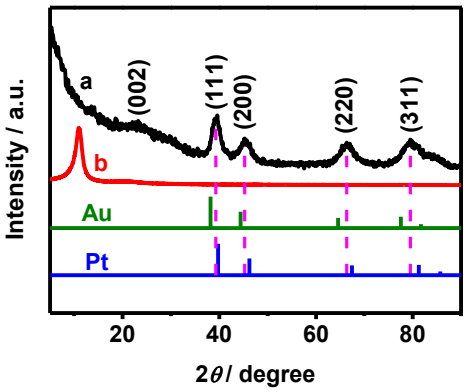

Fig. 3. XRD patterns of AuPt@Au NCs/rGO (curve a) and GO (curve b).

71.40 and 74.90 eV is originated from Pt^{2+}.[42] According to the relative peak intensities, we can easily say that metallic Au and Pt are the main species. In addition, the surface molar ratio of Pt to Au is about 1:3, which is lower than the EDS data, verifying the core-shell structure again.

A similar method is used to study the C 1s region. As illustrated in **Fig. 4D**, there are four peaks at 287.96, 286.43, 285.17 and 284.3 eV, assigned to O-C=O, C=O, C-O, and C-C (sp^2 C) groups,[43] respectively. One can see clearly that the peaks correlated with oxygen-functional groups are significantly lower than the C-C peak, indicating the efficient reduction of GO in the synthetic process.

Raman spectroscopy is a powerful technique to study carbon-based materials. As shown in **Fig. S3** (**SI**), there are two characteristic peaks emerged at 1326 (*D* peak) and 1595 cm^{-1} (*G* peak) for AuPt@Au NCs/rGO, which are associated with the disorder-activated Raman mode and the E_{2g} mode of graphite, respectively.[44, 45] In the case of GO (**Fig. S3**，**SI**), similar two dominate peaks are observed at 1359 (*D* peak) and 1608 cm^{-1} (*G* peak). The peak shifts between Pd@Pt DNC/rGO and GO are probably due to the interactions of the attached metallic catalysts with graphene.[46] In addition, the peak intensity ratio of the *D* to *G* band (I_D/I_G) is 1.17 for AuPt@Au NCs/rGO, which is higher than that of GO (0.96), demonstrating the reduction of GO and the decreased size of sp^2 domains of rGO.[45]

To determine the metal loading, thermogravimetric analysis (TGA) measurements were carried out from room temperature to 900 °C (**Fig. S4, SI**). All the samples undergo water evaporation, decomposition of oxygen moieties and destruction of carbon skeleton of rGO.[44] When the samples are heated to 700 °C, there are no significant mass losses observed, indicating the direct conversion of the residual mass to the metal loading in the samples. It is estimated that the metal loading is 81.7% for AuPt@Au NCs/rGO, 71.1% for Au/rGO and 37.3% for Pt/rGO, respectively.

3.2 Formation mechanism

Control experiments by the variation of melamine concentration were performed to illustrate the formation mechanism of AuPt@Au NCs/rGO (**Fig. S5, SI**). It is noticed that the absence of melamine yields numerous irregular

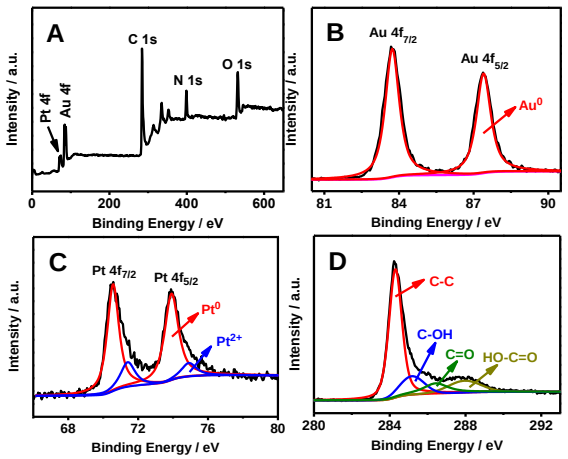

Fig. 4. Survey (A), high-resolution Au 4f (B), Pt 4f (C), and C1s (D) XPS spectra of AuPt@Au NCs/rGO.

nanoparticles deposited on rGO surface randomly. Alternatively, immature Au-Pt NCs emerge with un-uniform shapes at a relatively low melamine concentration (10 mM). And a lot of spherical nanoparticles with rough surfaces are clearly observed at 25 mM melamine, albeit with their poor quality. Increasing the melamine concentration to 50 mM produces well-defined spherical nanospheres with rough surfaces during the typical synthesis (**Fig. 1**). These results clearly demonstrate the crucial role of melamine in the present synthesis.

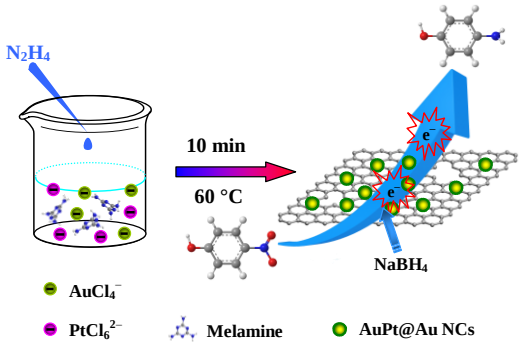

Fig. 5. Schematic illustration of the reduction of p-nitrophenol catalyzed by AuPt@Au NCs/rGO.

It is known that small adsorbates have the ability to control the morphology of metallic nanocrystals by selective adsorption on specific crystal planes.[47] **Fig. S6 (SI)** shows the schematic illustration of the formation process of AuPt@Au NCs. The metal precursors ($AuCl_4^-$ and $PtCl_6^{2-}$) are negatively charged, different from melamine containing three amino and

imino groups with positive charges. Thus, there are strong electrostatic interactions between the metal precursors ($AuCl_4^-$ and $PtCl_6^{2-}$) and melamine, forming melamine-$AuCl_4^-$ and melamine-$PtCl_6^{2-}$ composites. According to the previous reports about the reduction of the mixture of $PtCl_6^{2-}$ and $AuCl_4^-$ with a strong reducing agent,[48, 49] the reaction was very fast and AuPt nuclei showed up, instead of monometallic Au and Pt ones. In this case, numerous Au and Pt nuclei with high surface energy are generated and rapidly fused into AuPt nuclei after the addition of hydrazine hydrate as reducing agent. Afterward, the newly generated AuPt nuclei would be quickly capped by the adjacent melamine molecules. The metallic crystal growth is preferentially occurred on bare crystal planes, rather than the crystal planes occupied by melamine molecules, thanks to the selective adsorption ability.[50] The AuPt alloys are obtained via the epitaxial growth. On the other hand, the electrostatic interactions between the metal precursors and melamine have great effects on the reduction rate of the metal precursors in contrast with free metal salts under the identical conditions.[51, 52] Moreover, melamine-$PtCl_6^{2-}$ are firstly exhausted as compared to melamine-$AuCl_4^-$, followed by the reducing residual melamine-$AuCl_4^-$ to Au atoms. Thereby, exterior Au shell around inner AuPt core is emerged. It is probably due to the higher reduction rate of melamine-$PtCl_6^{2-}$ than that of melamine-$AuCl_4^-$.[42, 49] As a result, core-shell AuPt@Au NCs are formed on rGO via over-growth process. Melamine as a structure-director and stabilizing agent plays an important role in the formation of core-shell AuPt@Au NCs on rGO.

3.3 Catalytic reduction of p-nitrophenol

Herein, the reduction of *p*-nitrophenol with $NaBH_4$ in aqueous solution is chosen as a model reaction system to investigate the catalytic performance of AuPt@Au NCs/rGO, as depicted in **Fig. 5**. Typically, the aqueous *p*-nitrophenol solution exhibits pale yellow with the maximum absorbance at 317 nm. Upon the addition of $NaBH_4$, the solution immediately changes to greenish-yellow with the maximum absorption red shifted to 400 nm, owing to the formation of *p*-nitrophenolate ion in basic environment (**Fig. S7, SI**).[34, 53] After the addition of AuPt@Au NCs/rGO, the reaction solution color becomes fading and ultimately bleaches to colorless. Meanwhile, the peak intensity at 400 nm gradually decreases (**Fig. 6**), while a new peak appears at 300 nm, corresponding to *p*-aminophenol.[34, 53] Thus, the reaction kinetics can be easily monitored by measuring the adsorption at 400 nm as a function of time. The reaction time drops with the increasing dosages of AuPt@Au NCs/rGO because of the enlarged catalytic surface area.

On account of the large excess of $NaBH_4$ in this reduction media, the reaction rate is dependent on the concentration of *p*-nitrophenol. Thus, a pseudo-first-order rate kinetics can be assumed.[53] The apparent rate constant (k_{app}) is calculated by the following equation:[53, 54]

$$dC_t/dt = k_{app}\,t \quad \text{or} \quad \ln(C_t/C_0) = \ln(A_t/A_0) = k_{app}\,t$$

where C_0 and C_t are the *p*-nitrophenol concentrations at reaction time 0 and t, respectively. And A_0 and A_t are the absorbance at 400 nm at time 0 and t, respectively. Good linearity of $\ln(C_t/C_0)$ against time is obtained (**Fig. 6D**). The k_{app} is about 8.7 ×10^{-3} s^{-1} by using 0.05 mg of AuPt@Au NCs/rGO.

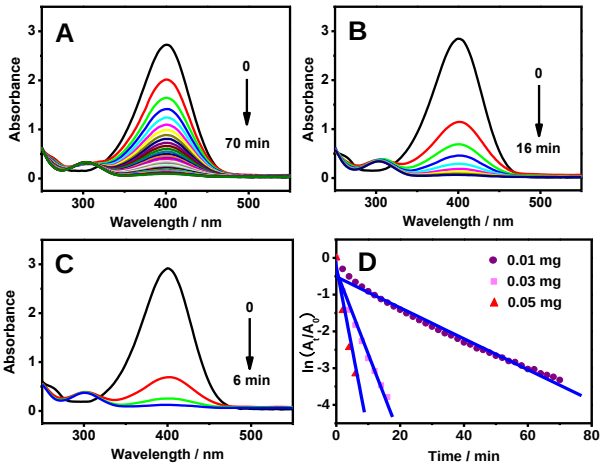

Fig. 6. Time-dependent UV-vis spectra of *p*-nitrophenol reduction catalyzed by different dosages of AuPt@Au NCs/rGO: 0.01 mg (A), 0.03 mg (B), and 0.05 mg (C). (D) Plots of the corresponding $\ln(A_t/A_0)$ against the reaction time.

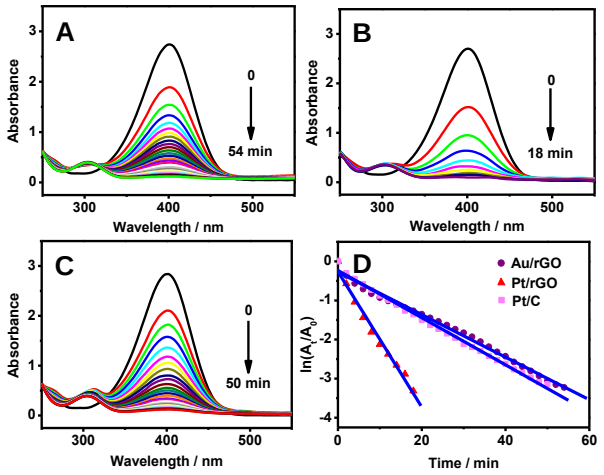

Fig. 7. Time-dependent UV-vis spectra of *p*-nitrophenol reduction catalyzed by 0.05 mg of Au/rGO (A), Pt/rGO (B), and Pt/C (C). (D) Plots of the respective $\ln(A_t/A_0)$ against the reaction time.

For comparison, the catalytic performances of Au/rGO, Pt/rGO and Pt/C catalysts were checked under the same situations. Similar spectral changes are observed, as shown in **Fig. 7**. It is found that the reaction time is much shorter for AuPt@Au NCs/rGO than the other two catalysts under the same conditions. The k_{app} values of Au/rGO, Pt/rGO and Pt/C are about 0.9 ×10^{-3}, 2.9 ×10^{-3} and 1.0 ×10^{-3} s^{-1}, respectively. Obviously, the k_{app} value is the highest for AuPt@Au NCs/rGO.

Meanwhile, the normalized rate constant (k_{nor}) is provided, which is correlated with the catalyst amount (m), i.e., $k_{nor} = k_{app}/m$.[54, 55] The k_{nor} of AuPt@Au NCs/rGO is 213 s^{-1} g^{-1}, which is larger than that of Au/rGO (25 s^{-1} g^{-1}), Pt/rGO (155 s^{-1} g^{-1}) and Pt/C (200 s^{-1} g^{-1}). Furthermore, this value is also larger than those of the catalysts reported previously such as carbon@Au core-shell nanofiber network (54.2 s^{-1} g^{-1}),[33] Pt-Au

alloy nanocubes (33 s^{-1} g^{-1}),[42] and Ag@Pd bimetallic hybrid (66.7 s^{-1} g^{-1}).[54] These results strongly verify the enhanced catalytic performance of AuPt@Au NCs/rGO toward *p*-nitrophenol reduction.

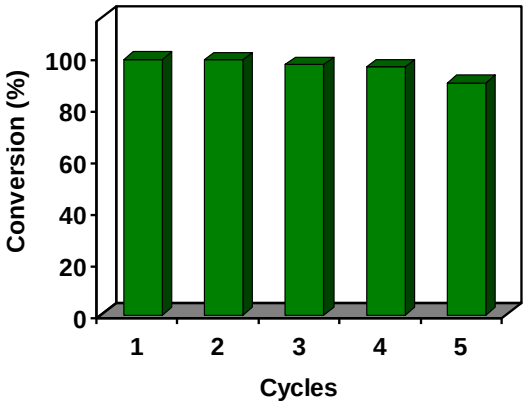

Fig. 8. The conversion yield of *p*-nitrophenol within 20 min by the repeated use of AuPt@Au NCs/rGO.

In order to explore the reusability of AuPt@Au NCs/rGO, the catalyst was recycled and utilized for the reduction of *p*-nitrophenol. **Fig. 8** displays the conversion of *p*-nitrophenol within 20 min with respect to five repeated cycles. It is observed that the conversion of *p*-nitrophenol slightly decreases, which is attributed to the limited aggregation and leaching of AuPt@Au NCs/rGO. As a result, AuPt@Au NCs/rGO has acceptable reusability and can be reused for at least 5 times, showing the potentials in practical applications.

In this reduction system, AuPt@Au NCs/rGO works as an electron relay system: electrons transfer from $NaBH_4$ to *p*-nitrophenol though AuPt@Au NCs. The improved catalytic performance of AuPt@Au NCs/rGO is mainly ascribed to the following respects: (i) Au has a low reaction rate because of its weak binding with *p*-nitrophenol, which means weak interactions with the reactants. However, alloying Au with Pt causes the stronger binding energy of Au shell for *p*-nitrophenol, significantly elevating the reaction rate.[56] (ii) rGO possesses high adsorption *via* π-π stacking interactions toward *p*-nitrophenol, resulting in concentrated *p*-nitrophenol molecules near AuPt@Au NCs on the support, thus increasing their efficient contacts.[33, 57] (iii) Electron transfer from rGO to AuPt@Au NCs takes place because rGO has a lower work function than Au, which causes an electron-enriched region, facilitating the uptake of electrons by *p*-nitrophenol.[57] (iv) rGO is benefit for the reactants adsorption and the electron transport for its enlarged surface area and excellent conductivity. In addition, the network-like structure of rGO stabilizes the immobilized AuPt@Au NCs, and prevents their aggregation and leaching during the catalytic process. All in all, the combination of Au, Pt and rGO endows positive effects on the catalytic reduction of *p*-nitrophenol by $NaBH_4$.

4. Conclusion

We have demonstrated a rapid one-step approach to prepare core-shell AuPt@Au NCs/rGO in aqueous media using melamine as structure-director and stabilizing agent. It was found that AuPt@Au NCs/rGO exhibited improved catalytic performance for the reduction of *p*-nitrophenol by $NaBH_4$ in aqueous solution, in contrast with Au/rGO, Pt/rGO and commercial Pt/C catalysts. The recyclability of the nanocomposites was acceptable. Therefore, the as-prepared catalyst is a promising material for practical applications in catalysis.

Acknowledgement

This work was financially supported by the National Natural Science Foundation of China (Nos. 21475118, 21175118, and 21275130).

Reference

1 J. Zhang, H. Yang, J. Fang and S. Zou, *Nano Lett.*, 2010, **10**, 638-644.
2 S. Alayoglu and B. Eichhorn, *J. Am. Chem. Soc.*, 2008, **130**, 17479-17486.
3 T. Mitsudome, Y. Mikami, H. Funai, T. Mizugaki, K. Jitsukawa and K. Kaneda, *Angew. Chem.*, 2008, **120**, 144-147.
4 J.-N. Zheng, L.-L. He, F.-Y. Chen, A.-J. Wang, M.-W. Xue and J.-J. Feng, *J. Mater. Chem. A*, 2014, **2**, 12899-12906.
5 J. Liu, S. Z. Qiao, J. S. Chen, X. W. D. Lou, X. Xing and G. Q. M. Lu, *Chem. Commun.*, 2011, **47**, 12578-12591.
6 X. Huang, Y. Li, Y. Chen, H. Zhou, X. Duan and Y. Huang, *Angew. Chem.*, 2013, **125**, 6179-6183.
7 F. Xiao, F. Zhao, D. Mei, Z. Mo and B. Zeng, *Biosens. Bioelectron.*, 2009, **24**, 3481-3486.
8 D. Y. Kim, K. W. Choi, X.-L. Zhong, Z.-Y. Li, S. H. Im and O. O. Park, *CrystEngComm*, 2013, **15**, 3385-3391.
9 Z. Wang, *J. Phys. Chem. B*, 2000, **104**, 1153-1175.
10 J. Gu, Y.-W. Zhang and F. F. Tao, *Chem. Soc. Rev.*, 2012, **41**, 8050-8065.
11 X. Liu, D. Wang and Y. Li, *Nano Today*, 2012, **7**, 448-466.
12 J. Huang, S. Vongehr, S. Tang, H. Lu and X. Meng, *J. Phys. Chem. C*, 2010, **114**, 15005-15010.
13 Y. Y. Chu, Z. B. Wang, J. Cao, D. M. Gu and G. P. Yin, *Fuel Cells*, 2013, **13**, 380-386.
14 C.-Y. Chiu, M.-Y. Yang, F.-C. Lin, J.-S. Huang and M. H. Huang, *Nanoscale*, 2014, **6**, 7656-7665.
15 B. Y. Xia, H. B. Wu, X. Wang and X. W. Lou, *J. Am. Chem. Soc.*, 2012, **134**, 13934-13937.
16 S. Wang and H. Xin, *J. Phys. Chem. B*, 2000, **104**, 5681-5685.
17 G. Fu, K. Wu, J. Lin, Y. Tang, Y. Chen, Y. Zhou and T. Lu, *J. Phys. Chem. C*, 2013, **117**, 9826-9834.
18 X. Kang, Z. Mai, X. Zou, P. Cai and J. Mo, *Anal. Biochem.*, 2007, **369**, 71-79.
19 F. Ye, H. Liu, W. Hu, J. Zhong, Y. Chen, H. Cao and J. Yang, *Dalton Trans.*, 2012, **41**, 2898-2903.
20 C. Neetzel, F. Muench, T. Matsutani, J. C. Jaud, J. Broetz, T. Ohgai and W. Ensinger, *Sens. Actuators, B*, 2015, **214**, 189-196.
21 A. A. Balandin, S. Ghosh, W. Bao, I. Calizo, D. Teweldebrhan, F. Miao and C. N. Lau, *Nano Lett.*, 2008, **8**, 902-907.
22 M. Katsnelson, K. Novoselov and A. Geim, *Nat. Phys.*, 2006, **2**, 620-625.

23 S. Stankovich, D. A. Dikin, G. H. Dommett, K. M. Kohlhaas, E. J. Zimney, E. A. Stach, R. D. Piner, S. T. Nguyen and R. S. Ruoff, *Nature*, 2006, **442**, 282-286.
24 F. Schedin, A. Geim, S. Morozov, E. Hill, P. Blake, M. Katsnelson and K. Novoselov, *Nat. Mater.*, 2007, **6**, 652-655.
25 P. Graphene, *Nano Lett.*, 2008, **8**, 3166-3170.
26 X. Wang, Y. Ouyang, X. Li, H. Wang, J. Guo and H. Dai, *Phys. Rev. Lett.*, 2008, **100**, 206803.
27 Y. Kim, Y. Noh, E. J. Lim, S. Lee, S. M. Choi and W. B. Kim, *J. Mater. Chem. A*, 2014, **2**, 6976-6986.
28 S.-S. Li, J.-N. Zheng, X. Ma, Y.-Y. Hu, A.-J. Wang, J.-R. Chen and J.-J. Feng, *Nanoscale*, 2014, **6**, 5708-5713.
29 S. Pandey and S. B. Mishra, *Carbohydr. Polym.*, 2014, **113**, 525-531.
30 Y.-P. Zhu, T.-Z. Ren and Z.-Y. Yuan, *RSC Advances*, 2015, **5**, 7628-7636.
31 Y.-P. Zhu, T.-Z. Ren and Z.-Y. Yuan, *Nanoscale*, 2014, **6**, 11395-11402.
32 K. B. Narayanan and N. Sakthivel, *Bioresour. Technol.*, 2011, **102**, 10737-10740.
33 P. Zhang, C. Shao, X. Li, M. Zhang, X. Zhang, C. Su, N. Lu, K. Wang and Y. Liu, *Phys. Chem. Chem. Phys.*, 2013, **15**, 10453-10458.
34 Z. Jiang, J. Xie, D. Jiang, X. Wei and M. Chen, *CrystEngComm*, 2013, **15**, 560-569.
35 P. Zhang, Y. Sui, G. Xiao, Y. Wang, C. Wang, B. Liu, G. Zou and B. Zou, *J. Mater. Chem. A*, 2013, **1**, 1632-1638.
36 W. S. Hummers Jr and R. E. Offeman, *J. Am. Chem. Soc.*, 1958, **80**, 1339-1339.
37 C.-M. Fan, L.-F. Zhang, S.-S. Wang, D.-H. Wang, L.-Q. Lu and A.-W. Xu, *Nanoscale*, 2012, **4**, 6835-6840.
38 J. Wang, G. Yin, H. Liu, R. Li, R. L. Flemming and X. Sun, *J. Power Sources*, 2009, **194**, 668-673.
39 W. Hong, J. Wang and E. Wang, *ACS Appl. Mat. Interfaces*, 2014, **6**, 9481-9487.
40 P. Zhang, R. Li, Y. Huang and Q. Chen, *ACS Appl. Mat. Interfaces*, 2014, **6**, 2671-2678.
41 D. Kim, Y. W. Lee, S. B. Lee and S. W. Han, *Angew. Chem. Int. Ed.*, 2012, **51**, 159-163.
42 G. Fu, L. Ding, Y. Chen, J. Lin, Y. Tang and T. Lu, *CrystEngComm*, 2014, **16**, 1606-1610.
43 Z. Fan, K. Wang, T. Wei, J. Yan, L. Song and B. Shao, *Carbon*, 2010, **48**, 1686-1689.
44 Y. Zhao, X. Song, Q. Song and Z. Yin, *CrystEngComm*, 2012, **14**, 6710-6719.
45 P. Cui, J. Lee, E. Hwang and H. Lee, *Chem. Commun.*, 2011, **47**, 12370-12372.
46 W. Wang, S. Liang, T. Yu, D. Li, Y. Li and X. Han, *J. Appl. Phys.*, 2011, **109**, 07C501.
47 A. R. Tao, S. Habas and P. Yang, *small*, 2008, **4**, 310-325.
48 S. Zhou, G. S. Jackson and B. Eichhorn, *Adv. Funct. Mater.*, 2007, **17**, 3099-3104.
49 C. Chu and Z. Su, *Langmuir*, 2014, **30**, 15345-15350.
50 A.-J. Wang, Y.-F. Li, M. Wen, G. Yang, J.-J. Feng, J. Yang and H.-Y. Wang, *New J. Chem.*, 2012, **36**, 2286-2291.
51 H. Zhu, S. Zhang, M. Li, Y. Shao and Z. Zhu, *Chem. Commun.*, 2010, **46**, 2259-2261.
52 S.-W. Kim, J. Park, Y. Jang, Y. Chung, S. Hwang, T. Hyeon and Y. W. Kim, *Nano Lett.*, 2003, **3**, 1289-1291.
53 X. Du, J. He, J. Zhu, L. Sun and S. An, *Appl. Surf. Sci.*, 2012, **258**, 2717-2723.
54 C.-H. Liu, X.-Q. Chen, Y.-F. Hu, T.-K. Sham, Q.-J. Sun, J.-B. Chang, X. Gao, X.-H. Sun and S.-D. Wang, *ACS Appl. Mat. Interfaces*, 2013, **5**, 5072-5079.
55 W. Ye, Y. Chen, F. Zhou, C. Wang and Y. Li, *J. Mater. Chem.*, 2012, **22**, 18327-18334.
56 Z. D. Pozun, S. E. Rodenbusch, E. Keller, K. Tran, W. Tang, K. J. Stevenson and G. Henkelman, *J. Phys. Chem. C*, 2013, **117** 7598-7604.
57 J. Li, C.-Y. Liu and Y. Liu, *J. Mater. Chem.*, 2012, **22**, 8426-8430.

Graphical Abstract

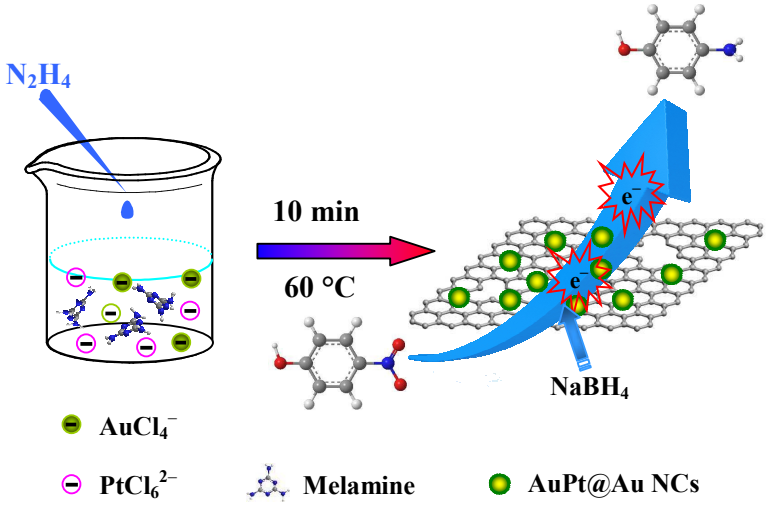

Core-shell AuPt@Au NCs/rGO was facilely prepared by a one-step melamine-assisted method, which exhibited enhanced catalytic performance for *p*-nitrophenol reduction.